Available online at www.sciencedirect.com
ScienceDirect
Journal of Applied Geophysics 64 (2008) 70–82
JOURNAL OF APPLIED GEOPHYSICS
www.elsevier.com/locate/jappgeo

Boundary element simulation of scattering of elastic waves by 3-D cracks

Ursula Iturrarán-Viveros [a,*], Francisco J. Sánchez-Sesma [b], Francisco Luzón [c]

[a] *Instituto Mexicano del Petróleo, Eje Central Lázaro Cárdenas 152, C.P. 07730, Mexico*
[b] *Instituto de Ingeniería, Universidad Nacional Autónoma de México, Cd. Universitaria, Circuito Escolar S/N, Coyoacán C.P. 04510, Mexico*
[c] *Universidad de Almería, Departamento de Física Aplicada, La Cañada de San Urbano 04120 Almería, Spain*

Received 24 June 2007; accepted 27 December 2007

Abstract

Numerical modelling techniques are now becoming common for understanding the complicated nature of seismic wave propagation in fractured rock. Here the Indirect Boundary Element Method (IBEM) is applied to study scattering of elastic waves by cracks. The problem addressed in this paper is the diffraction of *P* and *S* waves by open 3-D cracks of arbitrary shape embedded in a homogeneous isotropic medium. The IBEM yields the value of the jump of displacements between opposite surfaces of the crack, often called Crack Opening Displacement (COD). This is used to evaluate the solution away from the crack. We use a multi-regional approach which consists of splitting a surface S into two identical surfaces S^+ and S^- chosen such that the crack lies at the interface. The resulting integral equations are not hyper-singular and wave propagation within media that contain open cracks can be rigorously solved. In order to validate the method, we compare results of displacements of a penny-shaped crack for a vertical incident *P*-wave with the classic results by Mal (1970) obtaining excellent agreement. This comparison gives us confidence to study cases where no analytic solutions exist. Some examples of incidence of *P* or *S* waves upon cracks with various shapes are depicted and the salient aspects of the method are also discussed. Both frequency and time-domain results are included.

Keywords: Cracks; Scattering; Diffraction; Wave propagation; Boundary element method

1. Introduction

The scattering of elastic waves by cracks and other inhomogeneities is a long standing physical and mathematical problem. It has been of interest to geophysicists because it has many applications concerning the Earth's crust: underground storage, oil and gas prospecting and more generally investigation of the propagation of seismic waves in heterogeneous media. For example, in naturally fractured reservoirs changes in the physical properties can sometimes be explained by the extensive presence of empty or fluid-filled cracks and cavities. These features determine the pathways and volume of crustal fluid movements and can drastically change productivity in oil fields.

When analysing the phenomenology of elastic wave propagation in fractured rock one of the approaches consists of the assessment of the wave properties as the outcome of multiple scattering by a large number of individual fractures. In such considerations the scattering properties of each individual crack's edge, serve as building blocks in the future analysis, and for the theory to be successful, the knowledge of these properties in a manageable form is an indispensable prerequisite. For instance, using statistical hypothesis or equivalent media theories, diffraction patterns caused by many cracks can be deduced from that of a single crack (see Hudson, 1986).

Many results are already available for three dimensional crack analysis. Some of these include the earlier works by Mal (1968, 1970) where the author uses dual integral equations to compute displacements. Collected results by Tada et al. (1973), static solutions by Weaver (1977), Bui (1977), Mastrojannis et al. (1980), Murakami and Nemat-Nasser (1983), Lee and Keer (1982); dynamic solutions by Krenk and Schmidt (1982),

* Corresponding author.
E-mail addresses: uiturrar@imp.mx (U. Iturrarán-Viveros), sesma@servidor.unam.mx (F.J. Sánchez-Sesma), fluzon@ual.es (F. Luzón).

0926-9851/$ - see front matter © 2008 Elsevier B.V. All rights reserved.
doi:10.1016/j.jappgeo.2007.12.005

Angel and Achenbach (1984, 1985), Martin and Whickham (1983), Visscher (1985) and Lin and Keer (1986, 1987) are examples of various approaches used. Compared to domain methods, like finite-differences or finite-elements, boundary integral equation methods (BIE) have a conceptual advantage which is the reduction of one space dimension for both discretization and handling of the unknowns. This discretization gain is reinforced by the fact that the grid step sizes are larger than in domain methods. Other advantage is that these methods match easily the boundary conditions and do not suffer from grid dispersion. For crack diffraction problems, the boundary element method (BEM) or BIE is regarded as a natural choice because of its flexibility in defining the boundary cracks. It is also widely recognized as an effective modelling tool to solve problems in fracture mechanics (see Cruse, 1988). However, a number of difficulties present in the BEM formulation must be overcome in order to use it. The standard displacement-BIE formulation has been known to degenerate for crack problems (e.g. Cruse, 1978) since the displacements are allowed to be discontinuous on a single surface. This problem may be resolved through one of several approaches. One such approach consists of the use of dual boundary element method (Portela et al., 1992) which resolves the degeneracy by applying the traction-BIE on one of the crack surfaces. This approach is efficient in that it retains the displacement-BIE for much of the surface of the body, but hyper-singular integrals are introduced on the crack surface. Other approaches are used as in Rizzo et al. (1985), Bonnet (1995), Zhang and Gross (1998), Aliabadi (1997), Prosper (1998) and Prosper and Kausel (2001) where particular care is taken to regularize and solve the resulting integral equations. Here we choose instead the simpler Indirect Boundary Element Method (IBEM) that formulates the problem in terms of force densities which have to be obtained as an intermediate step. Perhaps, this is the reason why the IBEM is not as popular as the BEM in spite of the fact that these densities can give a deeper physical insight of diffracted waves. Moreover this approach is equivalent to that of Somigliana's representation theorem (see Sánchez-Sesma and Campillo, 1991) and can be regarded as a realization of the Huygens' principle. To deal with the crack we use sub-domains in which the cracked body is represented as two or more uncracked bodies with appropriate boundary conditions. This strategy implies that the non-physical boundaries generate extra unknowns increasing memory requirements, but with significant benefits. For instance, we may rigorously solve zero thickness cracks and choose to study any crack regardless its shape. This technique provides reliable results that can be used both to evaluate or to combine with other numerical techniques.

We assume mathematical cracks, therefore no contact between the faces of the crack is allowed and the crack tips are fixed. Thus, the cracks are linear and the material remains elastic everywhere. This approximation is enough to study diffracted waves. In fact, the cracks considered here act as scatterers and the asymptotic behaviour at the crack tip do not affect the radiated waves because of linearity. The crack tip stress concentrations, which are very important in fracture mechanics, reveal a local effect with little influence on the diffracted waves. It can be shown that the exact radiated waves depend upon an integral of the traction Green's tensor weighted by the COD and are somewhat insensitive to stress concentrations, see Sánchez-Sesma and Iturrarán-Viveros (2001). On the other hand, it is well known that high frequency waves are radiated if the crack tip propagates. Indeed, this radiation is controlled by variations in rupture velocity (Madariaga, 1976). This fact is very important in strong motion seismology, however it is beyond the scope of the present work. In the next section we proceed with the formulation of the problem. We explain how the multi-regional approach can lead to a single-layer integral representation without hyper-singularities. The multi-regional approach is somewhat different to the one used by Bonnet (1995). Therefore, numerical instability related to the interior problem if any, is avoided. In our formulation the domain in which we can obtain stable and accurate results is limited, but we can easily extend it by means of the Somigliana representation theorem (see for instance Achenbach, 1973; Aki and Richards, 1980; Banerjee and Butterfield, 1981). In order to validate our results we compare the solution obtained using the Indirect Boundary Element Method (IBEM) with the classical analytic solution by Mal (1970) for a penny-shaped crack. The validation of the IBEM for this problem enables us to use it confidently to solve problems where there are not known analytic solutions. Finally, in the last section we show and discuss some new numerical results for cracks of different shapes in both time and frequency domains.

2. Formulation of the problem

In crack scattering problems the total wave-field $\mathbf{u}^{(t)}$ is written as the superposition of the free field $\mathbf{u}^{(0)}$ (i.e. the reference field in the absence of scatterer) and the diffracted field $\mathbf{u}^{(d)}$ as follows:

$$\mathbf{u}^{(t)} = \mathbf{u}^{(0)} + \mathbf{u}^{(d)}. \tag{1}$$

Let us consider a Penny-shaped[1] crack under an incident plane wave as depicted on Fig. 1(a). The radius of the crack is taken as $a=1$, γ is the plane wave incident angle measured with respect to the z-axis and φ is the backazimuth measured with respect to the x-axis. Consider a surface extension at the crack's edge to form an auxiliary crack's neighbourhood. For flat cracks the surface extension is on the same plane, see Fig. 1(b) Other non-planar crack shapes may require special devices (e.g. splines) to construct the surface extension. These auxiliary surfaces are constructed finite and in practice can be relatively small. The smallest region we have used in the given examples for the crack's neighbourhood is a, half the crack's size. Then the surface in which the crack is embedded is divided into two identical and complementary 3-D sub-domains: S^+ and S^-. The illuminated surface S^+ is the one which is first struck by the

[1] We will consider cracks with other shapes, this is only to illustrate the procedure.

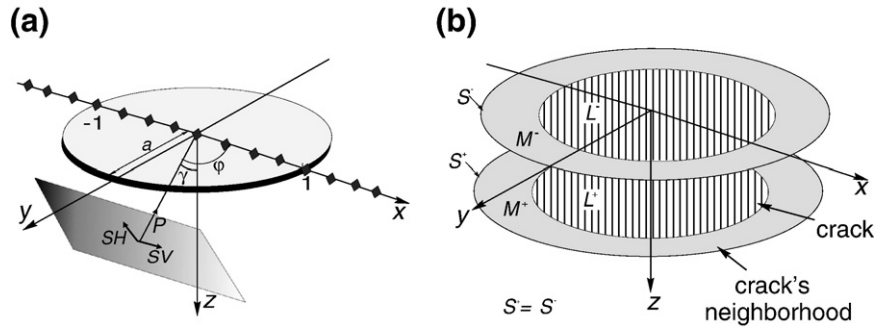

Fig. 1. (a) Penny-shaped crack under an incident plane wave. The radius of the crack is taken as a, γ is the plane wave incident angle measured with respect to the z-axis and φ is the backazimuth measured with respect to the x-axis. We consider *SH* and *P-SV* incident waves. (b) The surface in which the crack is embedded is divided into two complementary and identical 3-D sub-domains: S^+ and S^-. The illuminated surface is the one first stuck by the incident wave. We have assigned L number of nodes or elements to discretized the crack and M nodes to discretized the crack's elongation or neighbourhood. We discretized in the same way both surfaces S^+ and S^-.

incident wave, the shaded surface is denoted by S^-. The physics of the problem is given by suitable boundary conditions along S^+ and S^-. Particularly, we need to set continuity of displacements and tractions on the crack's elongation and zero tractions on the crack's faces. We propose to split the domain into two regions.

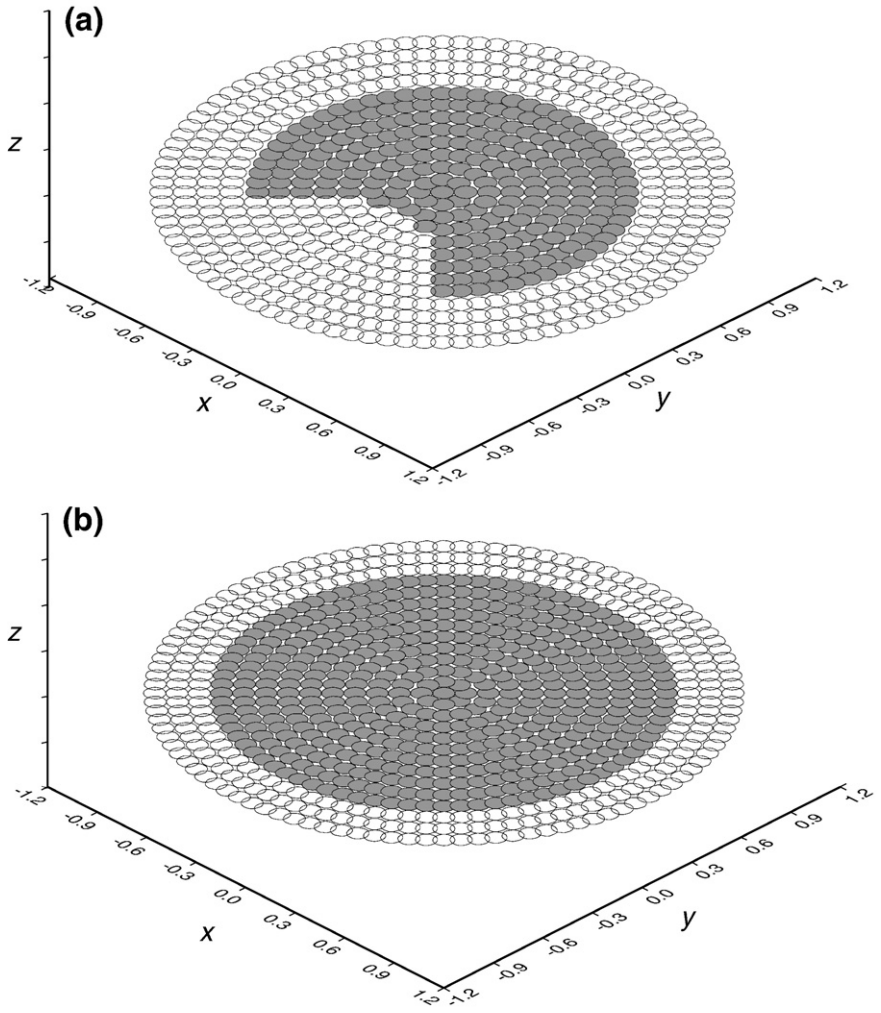

Fig. 2. (a) Discretization for the moon-shaped crack. We have 961 nodes from which 305 nodes are inside the crack and 656 discretize the elongation of the crack. (b) Similarly, we have the discretization for the penny-shaped crack with 961 nodes from which 441 are inside the crack and 520 outside.

Following Sánchez-Sesma and Campillo (1991) for each of the boundaries S^+ and S^-, the IBEM equations (with appropriate + or − superscripts) are:

$$u_i^{(d)}(\mathbf{x}) = \int_S \phi_j(\xi) G_{ij}(x,\xi) dS_\xi, \tag{2}$$

$$t_i^{(d)}(\mathbf{x}) = \pm\frac{1}{2}\phi_i(\mathbf{x}) + \int_S \phi_j(\xi) T_{ij}(\mathbf{x},\xi) dS_\xi \tag{3}$$

where (i, j=1,2,3) $u_i^{(d)}$ ($t_i^{(d)}$) is the diffracted displacement (traction) for a given $n_j(\mathbf{x})$; $G_{ij}(\mathbf{x}, \xi)$ ($T_{ij}(\mathbf{x}, \xi)$) is the displacement (traction) Green's function, i.e. the displacement (traction) at a point $\mathbf{x}$ (on a surface with a normal vector $n_{ij}(\mathbf{x})$) caused by a unit force at a point ξ; $\phi_j(\xi)$ is the force density at ξ and S is the corresponding S^+ or S^- boundary. The first term in (3) is for $\mathbf{x}\in S$ and the signs correspond to regions S^+ and S^- respectively. Further details are in Sánchez-Sesma and Luzón (1995). The integrals are computed along S. Exact formulations for both displacement and traction 3-D Green's functions are given by Sánchez-Sesma and Luzón (1995) and are included here in Appendix A.

Green's functions are singular when $\mathbf{x}=\xi$, but with appropriate discretization they can be integrated analytically using power series for the G and T terms. For a circle the integral of T, in the Cauchy principal value sense, is null. Moreover $G_{ij}(\mathbf{x}, \xi)$ on S^+ is identical to $G_{ij}(\mathbf{x}, \xi)$ on S^- since the two surfaces perfectly match. The same can nearly be stated for T when the unit normal vectors to S^+ and S^- are equal, the only difference being in the sign of the term outside the integral.

Let L and M be the number of elements considered to discretize, the crack and the associated neighbourhood, respectively. Then the total number of elements used to discretize both the crack and its neighbourhood is given by $N=L+M$. Boundary conditions at a point $\mathbf{x}$ on the crack are expressed by:

$$\frac{1}{2}\phi_i^+(x) + \int_S \phi_j^+(\xi_l) T_{ij}(x,\xi) dS_\xi = -t_i^{(0)+}(x), \tag{4}$$

$$-\frac{1}{2}\phi_i^-(x) + \int_S \phi_j^-(\xi_l) T_{ij}(x,\xi) dS_\xi = -t_i^{(0)-}(x), \quad l = 1,\ldots,L, \tag{5}$$

where the tractions $t_i^{(0)}$ are related to the incident wave field as follows. Given the incident field $u_i^{(0)}$ the tractions at a point $\mathbf{x}$ associated to a plane with normal $\mathbf{n}$ can be computed using Cauchy equations in terms of the stress tensor and the normal $\mathbf{n}$. This can be written as:

$$t_i^{(0)}(\mathbf{x}) = \sigma_{ij}^{(0)}(\mathbf{x}) n_j(\mathbf{x}) = c_{ijkl}\frac{\partial u_l^{(0)}(\mathbf{x})}{\partial x_k} n_j(\mathbf{x}) \tag{6}$$

where the stress tensor $\sigma_{ij}^{(0)}$ and displacement's gradient $\partial u_l^{(0)}/\partial x_k$ are related by the fourth order tensor $c_{ijkl}=\lambda\delta_{ij}\delta_{kl}+\mu(\delta_{ik}\delta_{ik}+\delta_{il}\delta_{ik})$, where λ and μ are the Lamé constants.

Boundary conditions of continuity of displacements and tractions at a point $\mathbf{x}$ on the crack neighbourhood are expressed by:

$$\int_S \left[\phi_j^+(\xi_l) - \phi_j^-(\xi_l)\right] G_{ij}(x,\xi) dS_\xi = 0, \tag{7}$$

$$\frac{1}{2}\left[\phi_i^+(x) + \phi_i^-(x)\right] + \int_S \left[\phi_j^+(\xi_l) - \phi_j^-(\xi_l)\right] T_{ij}(x,\xi) dS_\xi = 0, \quad l = L+1,\ldots,L+M, \tag{8}$$

where Eq. (7) corresponds to continuity of displacement and (8) defines continuity of traction. Eqs. (4), (5), (7) and (8) once discretized allow us to form a non-singular system for which there is a unique solution. Once the unknown force densities are found one can substitute them into Eq. (2), properly discretized, to obtain the displacement at any point $\mathbf{x}$ of the medium. However, the discretized zone is small and the accuracy could quickly deteriorate away from the crack. Therefore we should adopt a better strategy. Considering the full 3-D space domain and recalling Somigliana's identity in the frequency domain, we can write the following integral equation:

$$u_i^{(d)}(\xi) = \int_S \left[t_j^{(d)}(\mathbf{x}) G_{ij}(\mathbf{x},\xi) - u_j^{(d)}(\mathbf{x}) T_{ij}(\mathbf{x},\xi)\right] dS_\mathbf{x} \tag{9}$$

where ξ lies inside one of the sub-domains, $\mathbf{x}\in S$ and $S=S^+\cup S^-$. It is convenient that normal vector points away from the physical domain (as for S^+). This means that the normal at S^- should

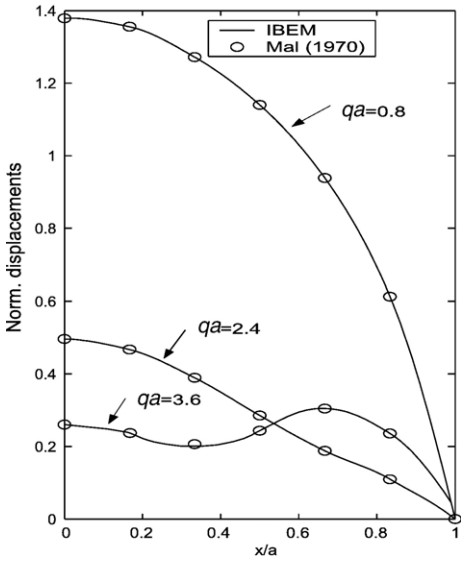

Fig. 3. A normal P wave is impinging upon a penny-shaped crack. The wave-numbers are qa=0.8, qa=2.4 and qa=3.6 respectively for each curve (being q the P-wave-number). Amplitude of the displacement calculated using Mal (1970) for this vertical incident P wave for three frequencies. The result is normalized to the displacement at the centre of the crack. Symbols correspond to Mal's solution and curves are IBEM results. We note a good agreement between the two solutions.

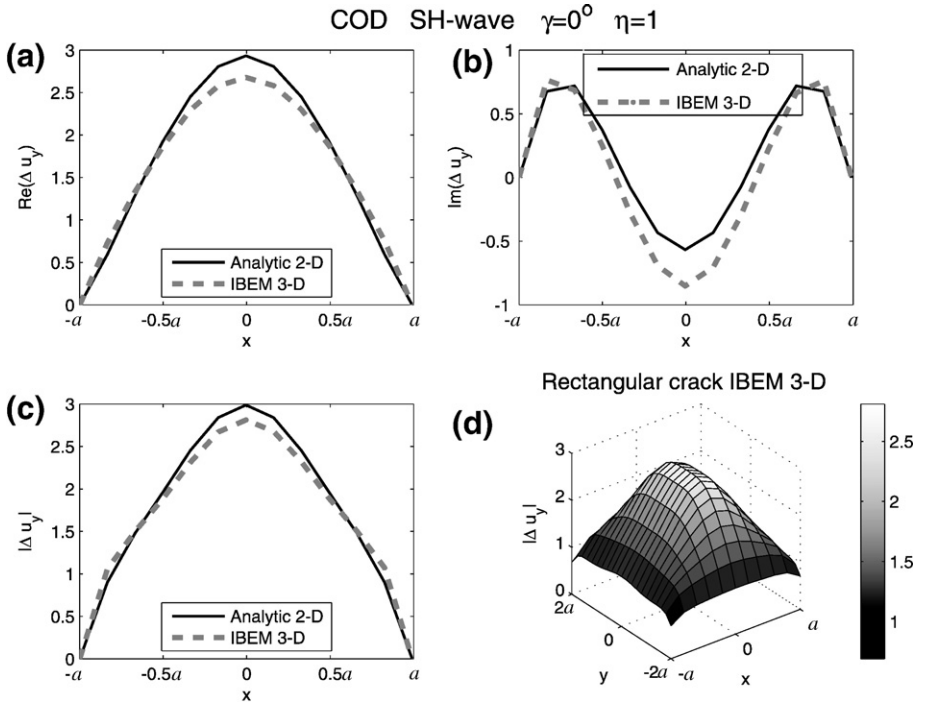

Fig. 4. (a) Real part of the COD at $y=0$ obtained numerically using IBEM for a 3-D rectangular crack of size ($2a\times4a$), normal incidence of *SH*-waves. The results are compared to a 2-D analytic solution for an infinite slit (see Sánchez-Sesma and Iturarán-Viveros, 2001). (b) Same as (a) but this is the imaginary part of COD. (c) Amplitude of COD at $y=0$ as in (a). (d) The COD obtained for a rectangular crack of and normal incidence of *SH*-waves with unit amplitude. Normalized frequency $\eta=\frac{\omega a}{\pi\beta}=1$. Results show good agreement although the differences are due to 3-D effects not considered by the 2-D analytic solution.

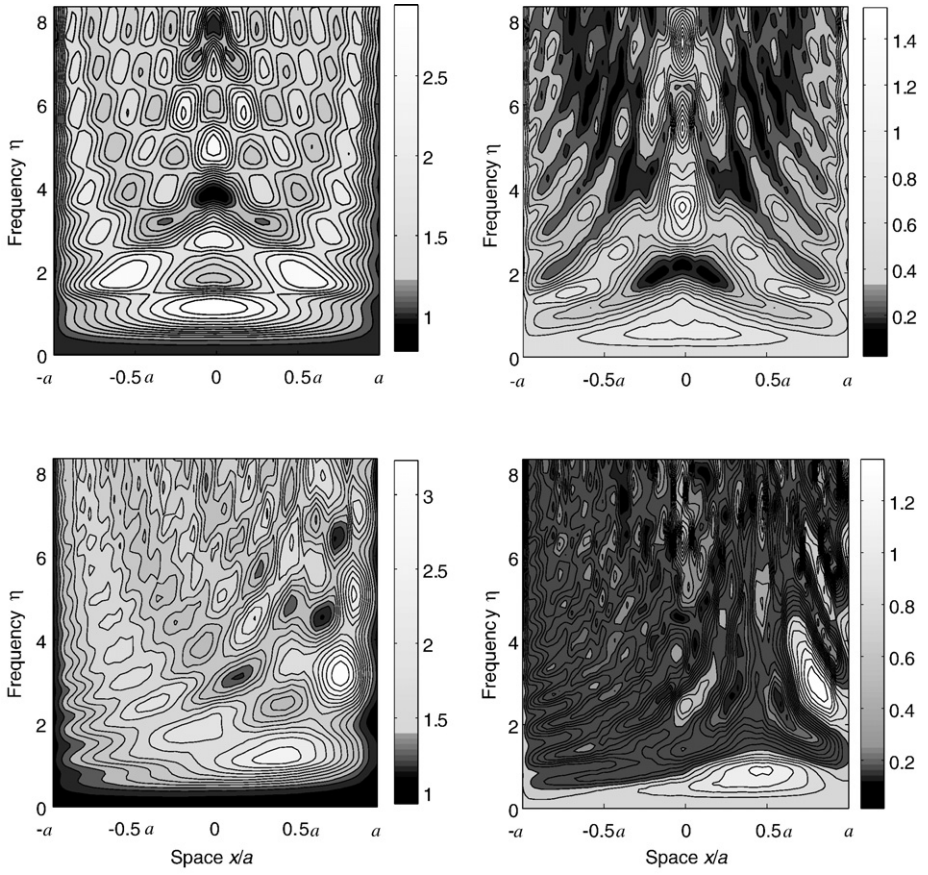

Fig. 5. Contour maps for a penny-shaped crack for incoming *SH*-waves with incidence angles $\gamma=0°$ (top) and $\gamma=30°$ (bottom), respectively, for both *illuminated* (left) and *shaded* (right) sides and backazimuth $\phi=0°$. This (**f-x**) diagram displays the total crack displacement amplitudes ($|u_y|$) along the crack sides against the normalized frequency $\eta=\frac{\omega a}{\pi\beta}$.

change direction. In that case diffracted and Green's tractions should satisfy:

$$\begin{aligned} t_i^{(d)+}(\mathbf{x}) &= -t_i^{(d)-}(\mathbf{x}), \qquad \mathbf{x}\in S \\ T_{ij}^{+}(\mathbf{x},\xi) &= -T_{ij}^{-}(\mathbf{x},\xi), \qquad \mathbf{x}\in S. \end{aligned} \tag{10}$$

Moreover, as the Green's functions $G(\mathbf{x},\xi)$ are independent of the normal vector definition, Eq. (9) can be rewritten as:

$$u_i^{(d)}(\xi) = \int_{S^+} \Delta u_j(\mathbf{x}) T_{ij}^{+}(\mathbf{x},\xi) dS_{\mathbf{x}} \tag{11}$$

where T^+ is the traction Green's function calculated accordingly to the unit normal vector pointing outward the illuminated space, and $\Delta \boldsymbol{u}_i(\mathbf{x}) = \boldsymbol{u}_i^+(\mathbf{x}) - \boldsymbol{u}_i^-(\mathbf{x})$ is the COD which is the displacement difference between the illuminated and shaded sides of the crack. The COD is null at the crack's neighbourhood. Unnecessary operations are cleared away and accuracy increases by using Eq. (11) instead of (9). In numerical applications there is an important benefit on the use of Somigliana's identity instead of the classical IBEM equations. S^+ and S^- should be infinite surfaces, but this is manifestly inconsistent with any numerical realization. The cutting of S is required at any effect. The numerical method we choose (the IBEM) can be seen as realization of the Huygens' principle: wave fronts are reproduced by radiating sources distributed along a surface. When S is cut, the set of sources along this boundary is interrupted and artificial diffraction at the edges is introduced. These spurious effects are not visible inside suitable space–time windows, depending on the length of S, the location of the observer and on wave speeds. In practice displacements along the crack can be calculated considering a short extension of S. By introducing the continuity conditions at the crack's neighbourhood, we are adding extra unknowns to the system of linear equations to be solved. In order to profit of the structure of the matrix, we could use sparse matrix computations (see Ortiz-Alemán et al., 1998). In this approach the IBEM is used to compute the COD which is the input of Somigliana's identity. Therefore, numerical noise is easily avoided and we obtain clean solutions at any point or time with low computational costs.

3. Numerical results

In this section we show a comparison between the results obtained using the IBEM and the classic results by Mal (1970) for a penny-shaped crack showing excellent agreement. This strongly suggest that our approach may give reliable results for cracks of arbitrary shape. Then we show numerical results for a rectangular crack, for a penny-shaped crack and for a moon-shaped crack in both time and frequency domains. In the next section we discuss details about discretization of the regions.

3.1. Discretization

In order to solve the resulting boundary integral equations we have to discretize them. In order to have the same number of

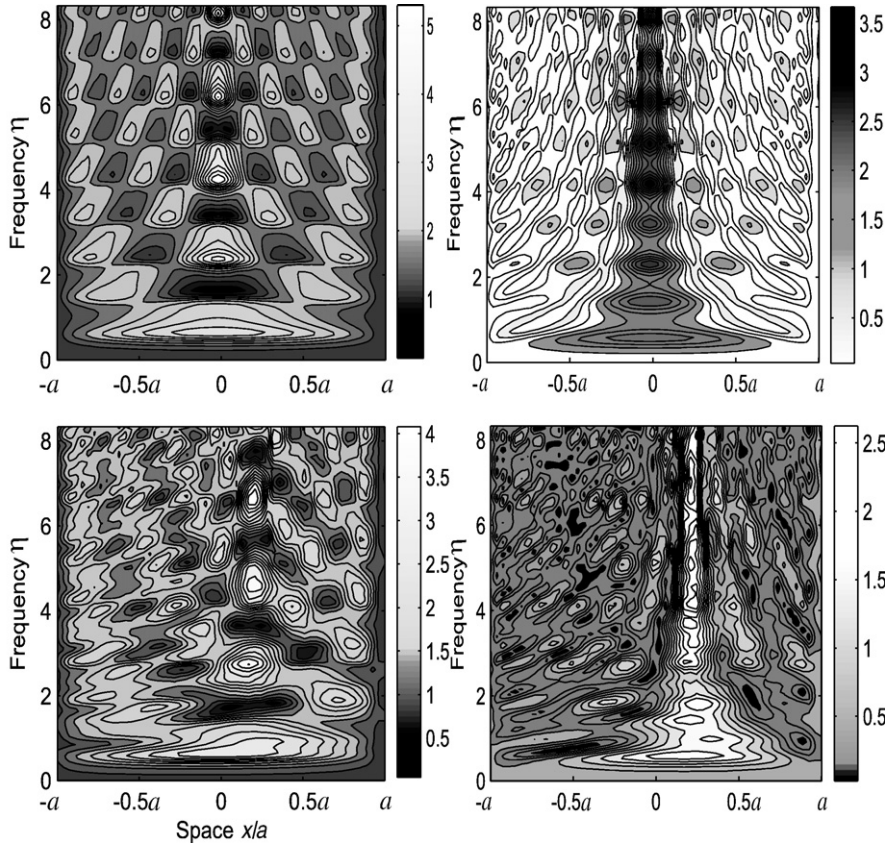

Fig. 6. This (f-**x**) diagram displays the total crack displacement amplitudes ($|u_z|$) along the crack sides against the normalized frequency $\eta = \frac{\omega a}{\pi \beta}$. Contour maps for a *P*-wave with incident angle $\gamma = 0°$ (top) and $\gamma = 30°$ (bottom) *illuminated* (left) and *shaded* (right) side.

equations and unknowns we may assume a set of regions and enforce boundary conditions. These boundary conditions are set at selected points, usually the centroids of each region. This is a feature that makes the IBEM to be regarded as a collocation method. The discretization of a surface is a well-known problem and several algorithms are available. In any case, the choice of discretization scheme depends upon the problem and the mathematical formulation to be used. For instance, in many applications, triangular elements are used to discretized surfaces (e.g. Manolis and Beskos, 1988; Brebbia and Dominguez, 1992; Yokoi and Sánchez-Sesma, 1998). In this work we choose a simplified scheme and discretize the surfaces using circles of various sizes that approximately cover the boundaries. Moreover, the force densities $\phi_i(\xi_l)$ are assumed to be constant over each circle. These might be regarded as crude choices. However, they allow us to keep the formulation simple and easy to implement. This is because the Green's functions on circles can be easily obtained in a closed form. Their contributions to the solution are computed by Gaussian numerical integration except in the case where the wave-field is evaluated on the source element itself. We have used four aligned elements per shortest wavelength. The surface S, the interface between the two sub-domains, is discretized using circles of the same size (though the sizes might vary, each one with surface ΔS_l and centre at ξ_l) that approximately cover the boundaries. Let L be the number of elements considered to discretize the crack and M the number of elements to discretize the neighbourhood of the crack. Then we have $3(2L+2M)$ equations which is the same number as the number of unknowns. This number corresponds to the three displacements in the illuminated and the shadow areas (here comes the factor of 2). Eqs. (4), (5), (7) and (8) allow us to form a non-singular system for which there is a unique solution. In order to clarify ideas, let us write the discretized version of Eqs. (2) and (3) as follows:

$$u_i(x) = \sum_{l=1}^{N} \phi_j(\xi_l) \int_{\Delta S_l} G_{ij}(x,\xi) dS_\xi \tag{12}$$

$$t_i(x_n) = \sum_{l=1}^{N} \phi_j(\xi_l) \left[\frac{1}{2}\delta_{ij}\delta_{nl} + \int_{\Delta S_l} T_{ij}(x,\xi) dS_\xi \right]. \tag{13}$$

The integral in Eq. (12) is computed numerically except in the case when $\mathbf{x}$ is in the neighbourhood of ξ_l for which we obtained analytical expressions. In particular, for $\mathbf{x}=\xi_l$, i.e. at the centre of a circle of radius R, it is possible to show that:

$$\int_{\Delta S_l} G_{ij}(\mathbf{x},\xi) dS_\xi = \frac{1}{4\mu}\left[(F_2+F_1)\delta_{ij} + (F_2-F_1)n_i n_j\right] \tag{14}$$

where F_k, $k=1, 2$ is simply the integral of f_k from 0 to R and $n_i=i$th component of the normal vector at the element. Functions f_k, $k=1, 2$ are defined by Eqs. (A.2) and (A.3) respectively. For $\mathbf{x}$ not in the centre we performed analytical

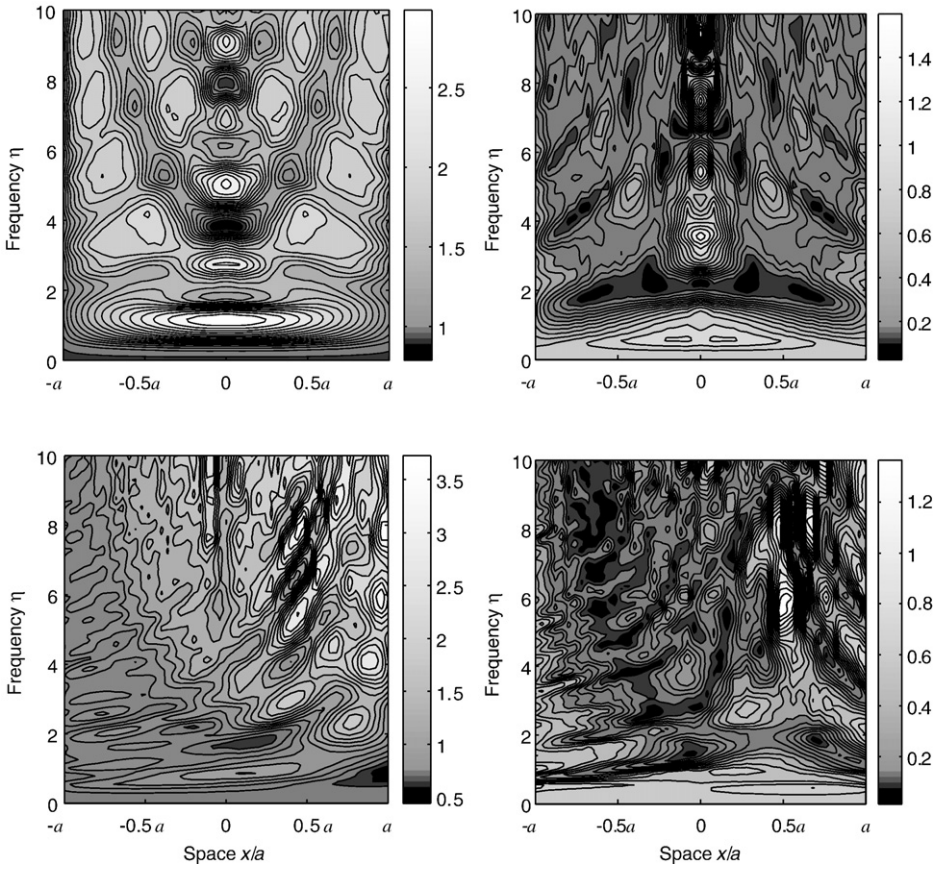

Fig. 7. This (f-$\mathbf{x}$) diagram displays the total crack displacement amplitudes ($|u_x|$) along the crack sides against the normalized frequency $\eta = \frac{\omega a}{\pi\beta}$. Contour maps for a *SV*-wave with incident angle $\gamma=0°$ (top) and $\gamma=30°$ (bottom) *illuminated* (left) and *shaded* (right) side.

integration in polar local coordinates and considered the ascending power series of f_1 and f_2. Up to cubic terms were retained and this is enough if the minimum wavelength is at least four diameters. The integral in Eq. (13) is also computed numerically except when $\mathbf{x}_n = \xi_l$. In this case we have:

$$\int_{\Delta S_n} T_{ij}(\mathbf{x}_n, \xi) d_\xi = 0, \tag{15}$$

because the contribution from the traction Green's tensor T_{ij} is null as long as the element is circular and flat, which is the case assumed here. Once the values of $\phi_j(\xi_l)$ are known, the scattered field is computed by means of the appropriated version of (12).

For the numerical simulations of scattering of elastic waves by a moon-shaped and a penny-shaped cracks we have used the discretizations shown in Fig. 2(a) and (b) respectively. In the case of a penny-shaped crack we have used 961 nodes from which 441 are inside the crack and 520 are to discretize the neighbourhood of the crack. For the moon-shaped crack we have used 961 nodes from which 305 nodes are inside the crack and 656 outside.

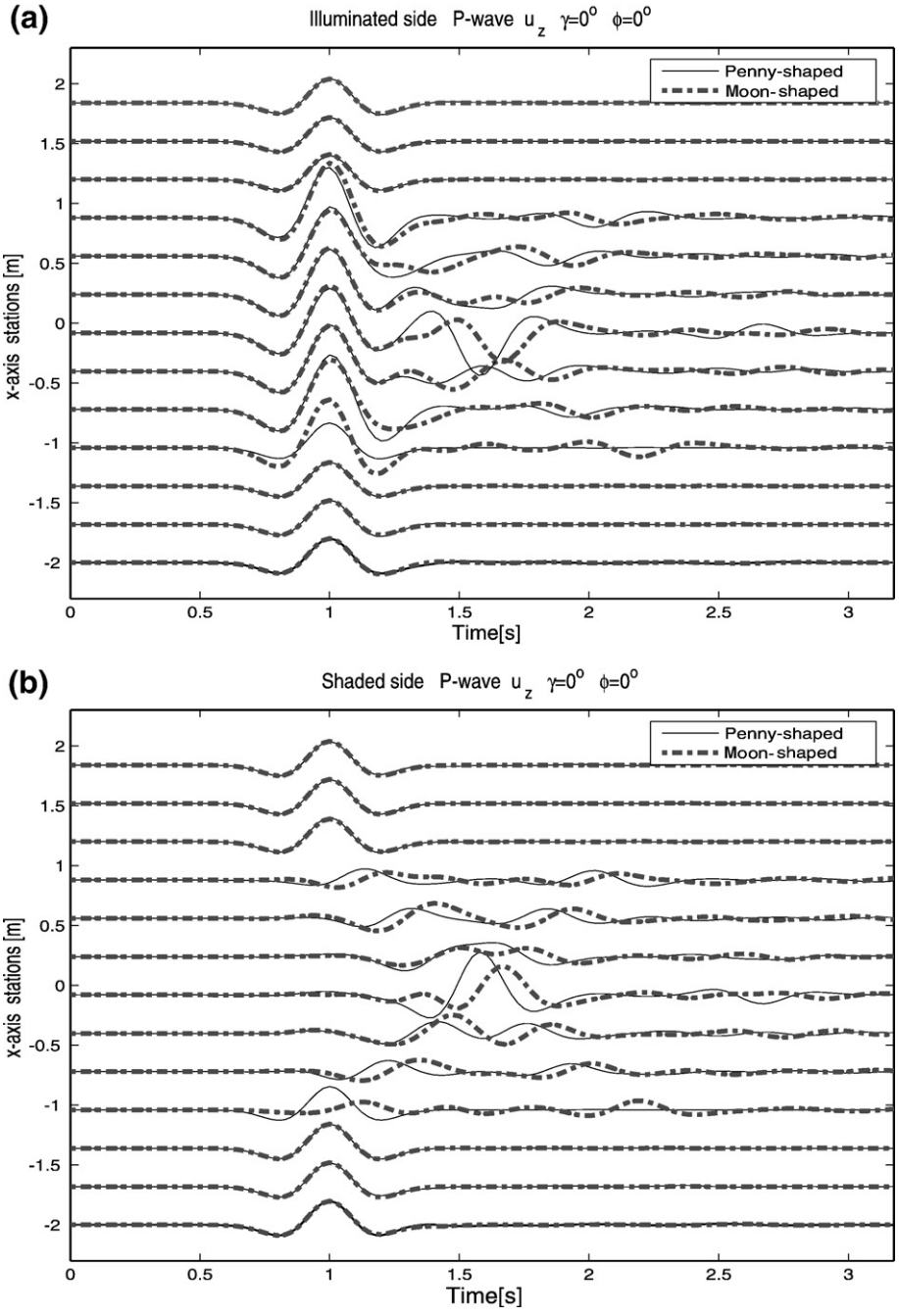

Fig. 8. Synthetic seismograms for a penny shaped and a moon-shaped cracks are computed from frequency-domain. The traces correspond to the total field for 13 equally spaced receivers. The first one is located at $x=-2a$ and with a spacing between them of $\Delta x=0.333a$ at $y=z=0.0$. Displacements u_z are shown on the (a) illuminated side of the crack and on the (b) shaded side of the crack.

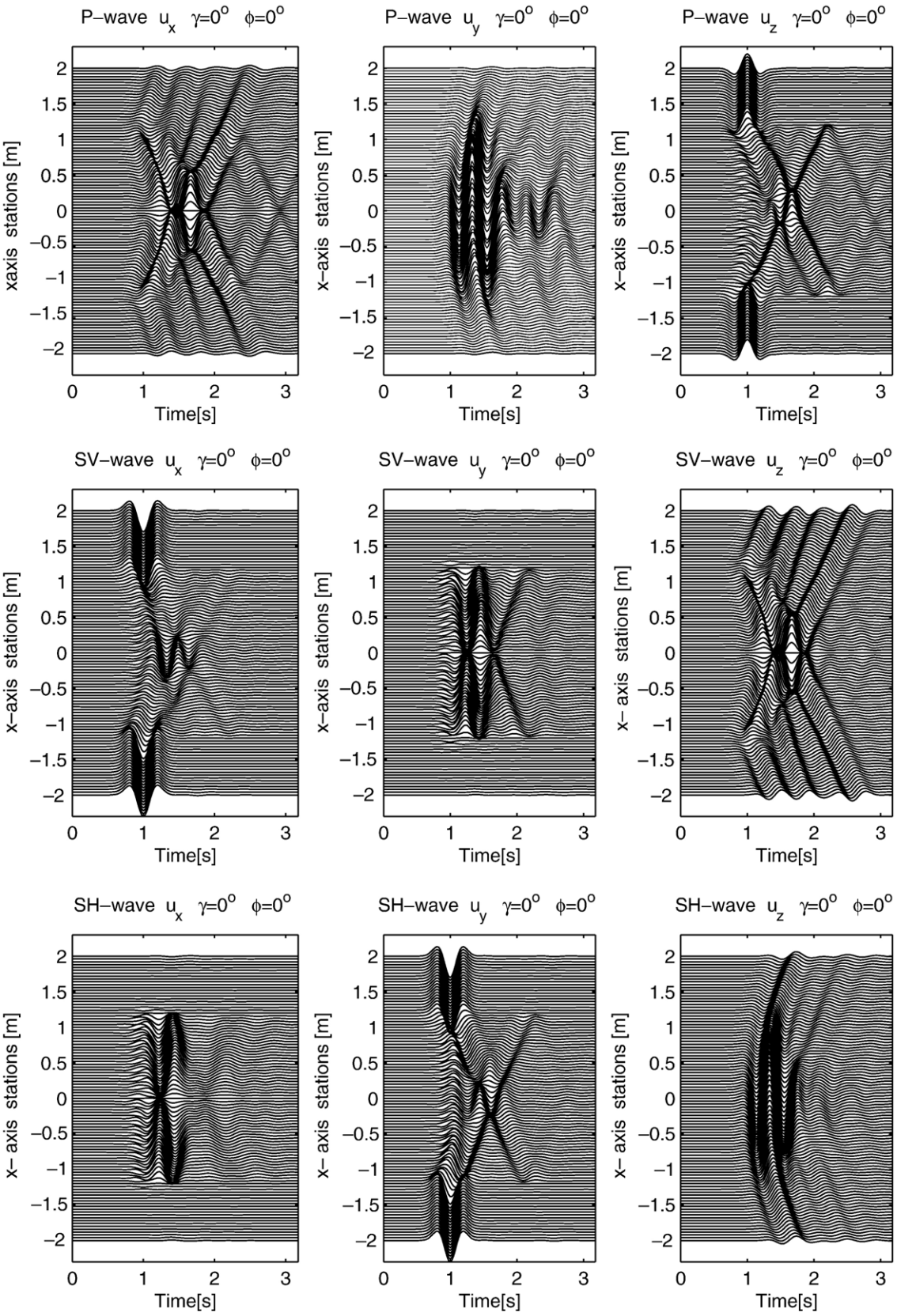

Fig. 9. Synthetic seismograms for a moon-shaped crack are computed from frequency-domain. The traces correspond to the total field for 101 equally spaced receivers located along the interval $x \in [-2a, 2a]$ at $y=z=0.0$. This case is for a *P*, *SV* and *SH* incident waves (top, middle and bottom, respectively). Displacements u_x, u_y and u_z are shown on the shaded side of the crack.

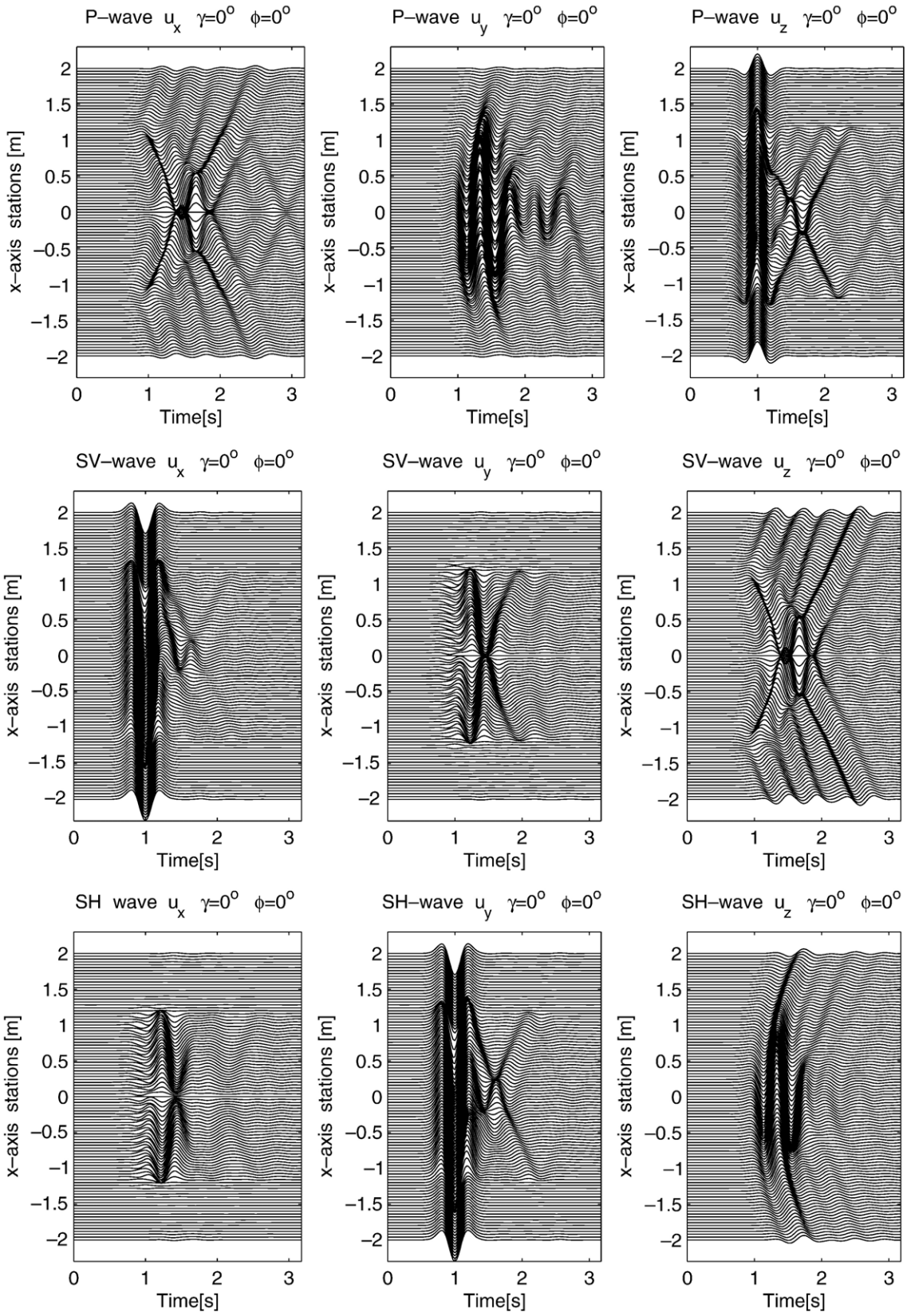

Fig. 10. Synthetic seismograms for a moon-shaped crack are computed from frequency-domain. The traces correspond to the total field for 101 equally spaced receivers located along the interval $x \in [-2a, 2a]$ at $y=z=0.0$. This case is for a P, *SV* and *SH* incident waves (top, middle and bottom, respectively). Displacements u_x, u_y and u_z are shown on the illuminated side of the crack.

3.2. Validation of the method

In a classic paper, Mal (1970) computed the crack opening displacement for various wavelengths of excitation using a dual integral equations for *P*-wave normally incident on a very thin crack located in an infinite elastic medium with radius a. Here we compare results obtained using the IBEM with those obtained by Mal. Let q be the *P*-wave number. The used parameters are $\mu=\rho=\beta=1$ (length units for ρ, β and a have to be in agreement) where β is the shear wave velocity given by $\beta=\sqrt{\frac{\mu}{\rho}}$, ρ is the density, μ is the shear modulus, the Poisson's ratio is $\nu=0.333$ and the wave-numbers are $qa=0.8$, $qa=2.4$ and $qa=3.6$ respectively for each curve depicted on Fig. 3. Excellent agreement has been found between our results and Mal's (1970). This is encouraging since it suggests that the numerical method can be used to deal with cracks of arbitrary shape.

We study the spectral response of a plane wave impinging upon a crack. Henceforth, we use a normalized frequency $\eta=\omega a/\pi\beta$, where ω is the circular frequency and a is the radius of the crack. We computed the COD for a rectangular crack ($2a\times 4a$) with normal incidence of a *SH* wave (motion along the y-axis, the largest side of the crack). Fig. 4 displays the COD $|\Delta u_y|$ for a normalized frequency $\eta=1$. We also display the COD at $y=0$ (the crack's centre, at half the largest side $4a/2$) and compare it with an analytic solution for a 2-D crack (see Sánchez-Sesma and Iturrarán-Viveros, 2001). The agreement is very good and it shows that, for the given frequency, the 3-D COD at the centre of a rectangular cracks almost match the behaviour of the slit.

Results on Fig. 5 correspond to contour maps for a penny-shaped crack for incoming *SH*-waves with incidence angles $\gamma=0°$ (top) and $\gamma=30°$ (bottom), respectively, for both *illuminated* (left) and *shaded* (right) sides and backazimuth $\phi=0°$. This (f-**x**) diagram displays the total crack displacement amplitudes ($|u_y|$) along the crack sides against the normalized frequency $\eta=8$. In Figs. 5 and 6 the receivers are located along the x-axis between $x\in[-a, a]$, being $\rho=\beta=1$ (length units for ρ, β and a have to be in agreement) and Poisson's ratio $\nu=0.333$.

Similarly on Fig. 6 we can see $|u_z|$ displacements for an impinging *P*-wave with incident angle $\gamma=0°$ and $\gamma=30°$ for both *illuminated* side (on the left) and *shaded* side (on the right). On Fig. 7 we plot $|u_x|$ contour maps for *SV*-waves with incident angle $\gamma=0°$ and $\gamma=30°$ for both *illuminated* side (on the left) and *shaded* side (on the right) and backazimuth $\phi=0°$. Note that $|u_x|$ for the *P*-wave and $|u_z|$ for the *SH*-wave are not included. The reason is that for an incident *P*-wave with $\gamma=0°$ we have that $|u_x|$ is the same for the illuminated and shaded sides. Similarly when we consider $|u_z|$ for an incident *SV*-wave we will have anti-symmetric results but we are considering the modulus $|u_z|$ so there will not be a difference between the shaded and the illuminated sides. Observe that for an *S*-wave with incident angle $\gamma=0°$ we will expect to see the same $|u_y|$ and $|u_x|$ along the y-axis. However, since we are plotting the displacements along the x-axis the results are different.

3.3. Penny-shaped and moon-shaped cracks

In this section we compare results obtained for a penny-shaped crack and for a moon-shaped crack. The results show the differences of the arrival times due to the different shape of the cracks. We construct the moon-shaped crack in such a way that it lies within a region for which the conditions $r<a$ and $R>b$ hold, where $r^2=x^2+y^2$ and $R^2=x^2+(y-a)^2$. In other words, it is limited by the intersection of two circumferences taking $b=0.65a$ and a being a length unit.

On Fig. 8 synthetic seismograms for a penny-shaped and a moon-shaped cracks are computed from frequency-domain results using the Fast Fourier Transform (FFT) algorithm. The traces correspond to the total field for 13 equally spaced receivers. The first one is located at $x=-2a$ and with a spacing between them of $\Delta x=0.333a$ at $y=z=0.0$. In Figs. 8 and 9 the incident time signal is a Ricker wavelet with characteristic period $t_p=0.5a/\beta$ and $t_s=2t_p$ where a is the radius of the crack. This case is for a *P* incident wave a Poisson's ratio of $\nu=0.333$, backazimuth $\phi=0°$, $\gamma=0°$ and $\rho=\beta=1$ (length units for ρ, β, and a have to be in agreement). Displacements u_z are shown on the (a) illuminated side of the crack and on the shaded side (b) of the crack. We can see that the difference between the arrival times are due to the difference in the shapes.

We show synthetic seismograms for a moon-shaped crack on Fig. 9 for the shaded side and on Fig. 10 for the illuminated side. The traces correspond to the total field for 101 equally spaced receivers located along the interval $x\in[-2a, 2a]$ at $y=z=0.0$. We can see in some cases the differences between the shaded and illuminated sides. For example, for an incident *SV*-wave the component u_x shows the clear difference between receivers located on the shadow, where there is no direct arrival and the direct arrival on receivers located on the illuminated side.

4. Conclusions

We have tested the IBEM to solve the problem of scattering of elastic waves by a 3-D open crack. The method was tested against the analytical solutions, for a canonical case, obtaining excellent agreement. By splitting the crack into two different domains, problems related to hyper-singularities have been overcome. The IBEM allows us to study media with arbitrary shaped cracks *SH* and *P-SV* wave scattering. More complex configurations of heterogeneities, fluid filled cracks or cavities can be dealt with using this technique and are currently being investigated. Computational costs increase with the frequency, this limits the resolution and is a serious constrain. However parallel computing for methods in the frequency domain is much simpler than time domain computation based on domain decomposition. This is an advantage of the IBEM and it will help to study more realistic problems in the near future. Numerical results are encouraging but further work is needed to be able to deal with the inverse problems. These results dealt with simple configurations because we regarded as building blocks of more complex configurations. The COD for various crack configurations have relatively simple behaviour and approximations may be devised to generate fast computational devices for multiple crack configurations.

Acknowledgments

We would like to thank keen comments from two anonymous reviewers that helped to improve the manuscript. This work has been partially supported by Programa de Exploración Petrolera from Instituto Mexicano del Petróleo. By DGAPA-UNAM México under grant IN114706. By the CICYT, Spain, under Grant CGL2005-05500-C02-02/BTE, by the European Commission with FEDER and by the Research Team RNM-194 of the Junta de Andalucía, Spain.

Appendix A. 3-D Green's functions in unbounded space

For an homogeneous isotropic elastic unbounded medium, the Green's function is due to Stokes (1849), see (Love, 1944). For harmonic time dependence $\exp(i\omega t)$, where $i^2=-1$, ω is the circular frequency and t is the time, the Green's tensor can be expressed in the following compact form:

$$G_{ij}(\mathbf{x},\xi) = \left[f_2\delta_{ij} + (f_1 - f_2)\gamma_i\gamma_j\right]/4\pi\mu r, \tag{A.1}$$

where $\gamma_j=(x_j-\xi_j)/r$, $r^2=(x_1-\xi_1)^2+(x_2-\xi_2)^2+(x_3-\xi_3)^2$. Here and in the sequel $\mu=\rho\beta^2$, $\lambda+2\mu=\rho\alpha^2$, being λ and μ the Lamé's constants, ρ the mass density, δ_{ij} the Kronecker's delta, $k=\omega/\beta$ the S-wave-number, $q=\omega/\alpha$ the P-wave-number, β and α the S and P wave velocities, respectively. We define f_1 and f_2 as follows:

$$f_1 = \frac{\beta^2}{\alpha^2}\left[1 - \frac{2i}{qr} - \frac{2}{(qr)^2}\right]exp(-iqr) + \left[\frac{2i}{kr} + \frac{2}{(kr)^2}\right]exp(-ikr) \tag{A.2}$$

$$f_2 = \frac{\beta^2}{\alpha^2}\left[\frac{i}{qr} + \frac{1}{(qr)^2}\right]exp(-iqr) + \left[1 - \frac{i}{kr} - \frac{1}{(kr)^2}\right]exp(-ikr), \tag{A.3}$$

which have constants 1 and $(1+(\beta/\alpha)^2)/2$, respectively, as limits if ω or r tend to zero. The corresponding Green's tractions are given by:

$$T_{ij} = \left[(g_1 - g_2 - 2g_3)\gamma_i\gamma_j\gamma_k n_k + g_3\gamma_i n_j + g_2\gamma_j n_i + g_3\gamma_k n_k\delta_{ij}\right]/4\pi r^2 \tag{A.4}$$

with functions $g_j, j=1, 2, 3$ expressed as:

$$g_j = \left[krA_{1j} + B_{1j} + \frac{C_{1j}}{kr} + \frac{D_{1j}}{(kr)^2}\right]exp(-ikr) + \left[krA_{2j} + B_{2j} + \frac{C_{2j}}{kr} + \frac{D_{2j}}{(kr)^2}\right]exp(-iqr). \tag{A.5}$$

The coefficients A, B, C, and D for this expression are given on the Table A. In Eqs. (A.1) and (A.4), Table A the usual summation convention for subscripts is assumed. Similar expressions for Green's functions have been presented by Auersch and Schmid (1990) using vector notation. Eqs. (A.1) and (A.4) allow a direct view of singularities at the point of application of the force. The singularity of displacements is $1/r$, this is clear from Eq. (A.1). Regarding the tractions, the singularity is explicitly of the form $1/r^2$. In particular, when frequency tends to zero, these equations lead to their static counterparts (see e.g. Love, 1944).

Table A
Coefficients for Eq. (A.5)

	j		
	1	2	3
A_{1j}	0	0	$-i$
A_{2j}	$-i\beta/\alpha$	$i(2\beta^3/\alpha^3-\beta/\alpha)$	0
B_{1j}	4	−2	−3
B_{2j}	$-4\beta^2/\alpha^2-1$	$4\beta^2/\alpha^2-1$	$2\beta^2/\alpha^2$
C_{1j}	$-12i$	$6i$	$6i$
C_{2j}	$12i\beta/\alpha$	$-6i\beta/\alpha$	$-6i\beta/\alpha$
D_{1j}	−12	6	6
D_{2j}	12	−6	−6

References

Achenbach, J.D., 1973. Wave propagation in elastic solids. Elsevier Science Publishers, Amsterdam.
Aki, K., Richards, P.G., 1980. Quantitative seismology, theory and methods. W. H. Freeman, San Fransisco.
Aliabadi, M.H., 1997. Boundary element formulations in fracture mechanics. Appl. Mech. Rev. 50, 83–96.
Angel, Y.C., Achenbach, J.D., 1984. Refection and transmission of obliquently incident Rayleigh waves by a surface-breaking crack. J. Acoust. Soc. Am. 75, 313–319.
Angel, Y.C., Achenbach, J.D., 1985. Stress intesity factors for 3-D dynamic loading of a cracked half-space. J. Elast. 15, 89–102.
Auersch, L., Schmid, G., 1990. A simple boundary element formulation and its application to wavefield excited soil-structure interaction. Int. J. Earthquake Eng. Struct. Dyn. 19, 931–947.
Banerjee, P.K., Butterfield, R., 1981. Boundary element methods in engineering science. McGraw Hill, London.
Bonnet, M., 1995. Boundary integral equation methods for solids and fluids. John Wiley & Sons, New York.
Brebbia, C.A., Domiguez, J., 1992. Boundary elements an introductory course, Boundary elements an introductory course, Comp. Mec. Publ, 2nd ed. Southampton & Mc Graw-Hill Book Co., New York.
Bui, H.D., 1997. An integral equation method for solving the problem of a plane crack of arbitrary shape. J. Mech. Phys. Solids 25, 29–39.
Cruse, T.A., 1978. Two dimensional BIE fracture mechanics analysis. Appl. Math. Model. 2, 287–293.
Cruse, T.A., 1988. Boundary elements analysis in computational fracture mechanics. Kluwer Acasemic Publishers, Boston U.S.A.
Hudson, J.A., 1986. A higher order approximation to the wave propagation constants for cracked solid. Geophys. J. Royal Astr. Soc. 87, 265–274.
Krenk, S., Schmidt, H., 1982. Elastic wave scattering by a circular crack. Phil. Tranc. R. Soc. Lond. A 308, 167–198.
Lee, J.C., Keer, L.M., 1982. Study of three-dimensional crack terminating at an interface. J. Appl. Mech. 53, 311–316.
Lin, W., Keer, L.M., 1986. Scattering by a horizontal subsurface penny-shaped crack. Proc. R. Soc. Lond. Ser. A 408, 277–294.
Lin, W., Keer, L.M., 1987. Scattering by a planar three-dimensional crack. J. Acoust. Soc. Am. 82, 1442–1448.
Love, A.E.H., 1944. A treatise on the mathematical theory of elasticity, fourth ed. Dover Publications, New York.
Madariaga, R., 1976. Dynamics of an expanding circular crack. Bull. Seis. Soc. Am. 66, 639–666.
Mal, A.K., 1968. Diffraction of elastic waves by a penny-shaped crack. Q, Appl. Math. 26, 231–238.

Mal, A.K., 1970. Interaction of elastic waves with Griffith crack. Int. J. Engng. Sci. 8, 763–776.

Manolis, G.D., Beskos, D.E., 1988. Boundary element methods in elastodynamics. Unwin Hyman Ltd., London.

Martin, P.A., Whickham, G.R., 1983. Diffraction of elastic waves by a penny-shaped crack: analytical and numerical results. Proc. R. Soc. Land. A 390, 91–129.

Mastrojannis, E.N., Keer, L.M., Mura, T., 1980. Growth of planar cracks induced by hydraulic fracturing. Int. J. Numer. Methods Eng. 15, 41–54.

Murakami, Y., Nemat-Nasser, S., 1983. Growth and stability of interfacing surface flaws of arbitrary shape. Eng. Fract. Mech. 17, 193–210.

Ortiz-Alemán, C., Sánchez-Sesma, F.J., Rodríguez, J.L., Luzón, F., 1998. Computing topographical 3D site effects using a fast IBEM/conjugate gradient approach. Bull. Seis Soc. Am. 88, 393–399.

Portela, A., Aliabadi, M.H., Rooke, D.P., 1992. The dual boundary element method: effective implementation for crack problems. Int. J. Numer. Methods Eng. 33, 1269–1287.

Prosper, D., (1998). Modeling and detection of delaminations in laminated plates. Ph. D. thesis, Massachusetts Institute of Technology.

Prosper, D., Kausel, E., 2001. Wave scattering by cracks in laminated media. In: Atluri, S., Nishioka, T., Kirkuchi, M. (Eds.), Advances in Computational Engineering and Sciences, Proc. ICCES'01, Puerto Vallarta México, Aug 19-25. TechScience Press.

Rizzo, F.J., Shippy, D.J., Rezayat, M., 1985. A boundary integral equation method for radiation and scattering of elastic waves in three dimensions. Int. J. Numer. Methods Eng. 21, 115–129.

Sánchez-Sesma, F.J., Campillo, M., 1991. Diffraction of P, SV and Rayleigh waves by topographic features: a boundary integral formulation. Bull. Seis. Soc. Am. 81, 2234–2253.

Sánchez-Sesma, F.J., Luzón, F., 1995. Seismic response of three-dimensional alluvial valleys for incident P, S and Rayleigh waves. Bull. Seis. Soc. Am. 85, 269–284.

Sánchez-Sesma, F.J., Iturrarán-Viveros, U., 2001. Scattering and diffraction of SH waves by a finite crack: an analytical solution. Geophys. J. Int. 145, 749–758.

Stokes, G.G., 1849. On the dynamic theory of diffraction. Trans. Camb. Phil. Soc. 9, 1–62.

Tada, H., Paris, P.C., Irwin, G.R., 1973. The stress analysis of cracks handbook, 1st ed. Del Research Corporation, St. Louis.

Visscher, W.M., 1985. Elastic waves scattering by a surface-breaking or subsurface planar crack II. Three dimensional geometry. J. Appl. Phys. 57, 1538–1550.

Weaver, J., 1977. Three dimensional crack analysis. Int. J. Numer. Methods. Eng. 13, 321–330.

Yokoi, T., Sánchez-Sesma, F.J., 1998. An hybrid calculation technique of the indirect Boundary Element Method and the analytical solutions for three-dimensional problems of topography. Geophys. J. Int. 133, 121–139.

Zhang, C.H., Gross, D., 1998. On wave propagation in elastic solids with cracks, 1st ed. Computational Mechanics Publications, Southamptom, U.K.